



Facile synthesis: from *Laminaria hyperborea* to cellulose films and fibers

Yanqi Dai · Dongyang Sun · Senthilarasu Sundaram · Angelo Delbusso · Dominic O'Rourke · Mark Dorris · Mohan Edirisinghe

Received: 14 March 2023 / Accepted: 8 November 2023 / Published online: 1 December 2023
© The Author(s) 2023

Abstract Inverted nozzle-pressurized gyration was used as a processing methodology for regenerating cellulose extracted from *Laminaria hyperborea* for the first time. The viscoelasticity of cellulose/1-ethyl-3-methylimidazolium acetate (EMIM OAc) solutions exhibited high concentration dependence, leading to the production of cellulose products with diverse structures. The regenerated cellulose transitioned from thin films to fibers ($\approx 5 \mu\text{m}$ diameter) as the concentration was increased. The impact of collection distance and working pressure on the morphology and yield of fibers was investigated. This work provides a new sustainable route for processing biopolymers, offering significant potential for applications in biomedicine and healthcare.

Keywords Cellulose · Fibers · Pressurized gyration · Biopolymers · Sustainability

Introduction

In light of the increasingly urgent challenges posed by rising demands for raw materials and environmental pollution, cellulose has garnered significant attention as a promising alternative to synthetic polymers (Lin and Dufresne 2014) and has vast potential for the development of value-added products. Despite some success that has been reported (Quan et al. 2010; Sayyed et al. 2019; Zhuang et al. 2012), the secondary processing and scale-up of cellulose materials remain a major challenge. Cellulose is insoluble in water and most organic solvents due to the strong inter and intra-molecular hydrogen bonds (Seddiqi et al. 2021). Chemical derivatization (Klemm et al. 2005) and direct solvent systems, such as *N*-methylmorpholine *N*-oxide (NMMO) and lithium chloride/*N,N*-dimethylacetamide (LiCl/DMAc) (Fink et al. 2001; McCormick et al. 1985), are typical strategies for cellulose dissolution. However, cumbersome processes, thermal instability, and harmful by-products are significant drawbacks of these methods. Recently, imidazolium-based ionic liquids attracted attention due to their excellent ability to dissolve cellulose without any pre-activation (Pinkert et al. 2009; Wang et al. 2012). Ionic liquids dissolve cellulose by forming hydrogen bonds with the hydroxyl groups of

Supplementary Information The online version contains supplementary material available at <https://doi.org/10.1007/s10570-023-05606-w>.

Y. Dai · A. Delbusso · M. Edirisinghe (✉)
Department of Mechanical Engineering, University
College London, London, UK
e-mail: m.edirisinghe@ucl.ac.uk

D. Sun · D. O'Rourke · M. Dorris
School of Computing Engineering and the Built
Environment, Edinburgh Napier University, Edinburgh,
UK

S. Sundaram
School of Computing, Engineering and Digital
Technologies, Teesside University, Middlesbrough, UK

cellulose and both anions and cations are involved in this process (Salama and Hesemann 2020; Wang et al. 2012; Zhu et al. 2006). The advantages of ionic liquids as solvents for cellulose and other biomass are enormous, including chemical and thermal stability, non-flammability, low vapor pressure, and excellent solvency (Sescousse et al. 2010; Zhu et al. 2006). In addition, ionic liquids are considered green solvents (Holbrey and Seddon 1999) and can be recycled for reuse. Various methods can be used to recover the ionic liquid, for example, liquid-liquid extraction (Handy and Zhang 2001), supercritical CO₂ separation (Wu et al. 2009), and membrane separation (Haerens et al. 2010), depending on the ionic liquid used and their applications. 1-Butyl-3-methylimidazolium chloride (BMIMCl), 1-ethyl-3-methylimidazolium acetate (EMIM OAc), and 1-allyl-3-methylimidazolium chloride (AMIMCl), etc. have been used for cellulose dissolution (Elschner et al. 2014; Li et al. 2009; Liu et al. 2013; Pinkert et al. 2009; Wang et al. 2011). Such an effective dissolution of cellulose can be utilized to process synthetic cellulose fibers as alternatives to viscose and Lyocell in textile industries (Michud et al. 2016).

Nozzle-pressurized gyration (nozzle-PG) is one of the latest advanced technologies for the mass production of polymeric fibers, and has vast potential in the manufacturing of highly uniform and aligned fiber mats. Nozzle-PG combines the features of forcespinning and solution blowing, driving a gyrospun nozzle vessel with a high-speed electrical motor. The polymer fluid with sufficient viscosity forms spinning jets under the multi-action of centrifugal force and pressure difference. The spinning jet, once ejected, continues to stretch along the vessel circumference in the air, with the fiber dimension influenced by multiple factors. Typically, the increased viscoelasticity of spinning fluid, the heightened working pressure, and the longer collecting distance play roles in the additional stretching and fining of the produced fibers (Dai et al. 2023). After the evaporation of the solvent, dried fibers are deposited on the collector located at a specific distance. The fibers produced through this technology are typically non-woven long fibers. In nozzle-PG, the high working pressure facilitates the elongation and thinning of the spinning jets, as well as solvent evaporation, achieving the production of finer fibers (Mahalingam and Edirisinghe 2013). The external nozzles reduce the kinetic instability of

polymer jets to produce more uniform fibers. Highly controllable processing parameters, such as rotational speed, working pressure, collection distance, relative humidity, and temperature, make nozzle-PG very promising for fiber customization (Heseltine et al. 2018). The superiority of producing synthetic polymer fibers by nozzle-PG has been reported in a previous study (Dai et al. 2022). Nozzle-PG is notable for its capability in large-scale fiber production, offering a brighter prospect for amplifying cellulose fiber output than traditional wet spinning. Moreover, the elevated working pressure within nozzle-PG is beneficial in handling the highly viscous cellulose/ionic liquid solutions, as well as provides additional stretching of spinning jets. Consequently, this novel spinning method targets a more streamlined and efficient production of fine cellulose fibers.

This work provides a new efficient route to regenerated cellulose fibers by nozzle-PG. *Laminaria hyperborea* was used as the resource for deriving cellulose. The cellulose extract obtained was dried and dissolved in an ionic liquid (EMIM OAc) to prepare spinnable cellulose solutions. Dimethyl sulfoxide (DMSO) was used as the cosolvent. This has been reported to be a good cosolvent for cellulose dissolution in ionic liquids (Durmaz and Çulfaz-Emecen 2018). Inverted nozzle-PG invented here was used to spin the cellulose solutions into a water coagulation bath under a specific rotational speed and working pressure, forming gel-like cellulose. The cellulose samples spun from cellulose solutions with different concentrations exhibit different structures after washing and drying. This study proposes a novel and efficient method for preparing polymer fibers/films from natural materials, making a significant contribution to the development of biopolymers.

Experimental details

Materials

Cellulose extracted from Sugar Kelp (*Laminaria hyperborea*) was provided by Marine Biopolymers Ltd, UK. The seaweed cellulose is a by-product of alginate production which is solubilized and extracted leaving the insoluble cellulose fraction behind. The cellulose is naturally pure, free from lignin and hemicellulose and the received material

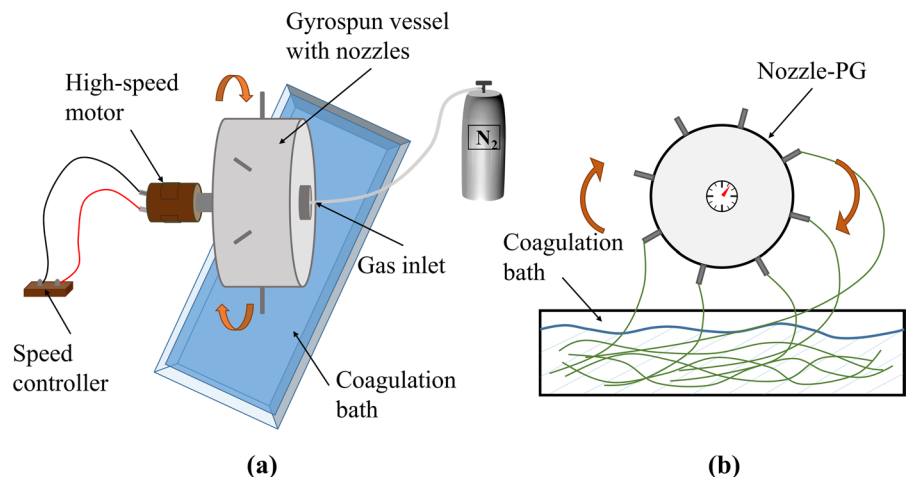
was washed thoroughly to remove any remaining soluble fractions and residual salts from the alginate extraction process. The material was subjected to high-pressure homogenization without any further pretreatment following the procedure of Onyianta et al. (2020), resulting in high aspect ratio cellulose nanofibrils. The average fibril width is 19 ± 5 nm. Fibril length could not be determined accurately due to the inherent length of the fibrils but is estimated, using low-res magnification SEM, to be in the order of several micrometers long, resulting in an aspect ratio greater than 100. Subsequently, free-flowing cellulose powder was prepared by a series of solvent exchange, filtration, and drying steps. The degree of polymerization (DP) of the cellulose obtained was characterized as 309. 1-Ethyl-3-methylimidazolium acetate (EMIM OAc, CAS: 143314-17-4) and dimethyl sulfoxide (DMSO, CAS: 67-68-5) were obtained from Sigma-Aldrich UK. A mixture of EMIM OAc and DMSO with a weight ratio of 1:1 was used to dissolve *Laminaria hyperborea* cellulose. The dissolving process was aided by repetitive oven heating and vigorous mixing using an acoustic mixer (LabRAM, Resodyn, USA) until the cellulose was completely dissolved to form a homogeneous solution. By exploring the spinnability of a series of cellulose solutions, the solutions with concentrations of 2 wt%, 2.5 wt%, and 3 wt% were used as the spinning feed materials in this work. The surface tension and viscosity of the prepared solutions were characterized at ambient temperature by a calibrated Kruss Tensiometer and a Brookfield Viscosity-meter, respectively. Each measurement was

replicated three times to determine the average and standard deviation values. Phosphate buffer saline (PBS, pH=7.4) was purchased from Oxoid ThermoFischer, UK.

Inverted nozzle-pressurized gyration

It was found from the experiments that the spinning jets cannot form a structured entity before being collected when the cellulose solutions were spun with a typical nozzle-PG device (Dai et al. 2022). Since ionic liquids are non-volatile solvents, they are not suitable for traditional dry spinning. Therefore, a nozzle-PG setup was modified to introduce a coagulation bath used in the wet spinning of cellulose solutions. In this study, inverted nozzle-PG was used to process the cellulose solutions. This setup is shown in Fig. 1a. A gyrosun vessel incorporated with 8 nozzles was driven by an electrical motor that can reach a rotational speed of 12,000 rpm. A gas inlet was connected to the vessel to provide a working pressure of up to 0.3 MPa. A water coagulation bath was introduced into the nozzle-PG setup (Fig. 1b). The cellulose solutions prepared were drawn into the water coagulation bath after emerging from the device. The minimum vertical distance between the water surface and the nozzle tip was 6–20 mm. The rotational speed was consistent (12,000 rpm) and the working pressure was 0.1–0.2 MPa. All experiments were performed at ambient temperature (~ 22 °C), 55% relative humidity, and repeated three times.

Fig. 1 **a** Schematic and **b** front view of the inverted nozzle-PG setup with a coagulation bath. Video clips of the process are given in Supplementary Information (SI1)



Preparation of cellulose fibers/films

Cellulose solutions (Fig. 2a) spun by nozzle-PG coagulated in the water bath at the ambient temperature. The resulting cellulose samples were immersed in the coagulant for 5 h (Fig. 2b). The coagulant was replaced every hour to wash the remaining ionic solvent properly. After sufficient coagulation and washing processes, the gel-like cellulose wet membranes (Fig. 2c) were removed from the coagulant. After pre-drying with an absorbent tissue at the ambient temperature, the moist cellulose membranes (Fig. 2d) were dried in the oven at 55 °C overnight. Eventually, dried cellulose fibers (Fig. 2e) and cellulose films (Fig. 2f) were obtained from the cellulose solutions with different concentrations. The weight of the moist cellulose samples and the dried samples were measured.

Field emission scanning electron microscopy (FE-SEM)

The morphology of the cellulose fibers/films was examined using a GeminiSEM 360 (ZEISS, Germany). The samples were observed with the FE-SEM at 3 kV acceleration voltage. On the obtained SEM images, the diameters of 100 randomly selected fibers were measured using ImageJ (software) to calculate the average fiber diameter. The fiber diameter distributions were plotted using OriginPro (software).

Fourier transform infrared spectroscopy

The chemical composition of the cellulose fibers/films was analyzed using a Fourier transform infrared spectroscopy (FTIR) spectrometer (Thermo Scientific Nicolet Is50) at ambient temperature. Each cellulose sample was scanned for 32 rounds between 4000 and 500 cm^{-1}

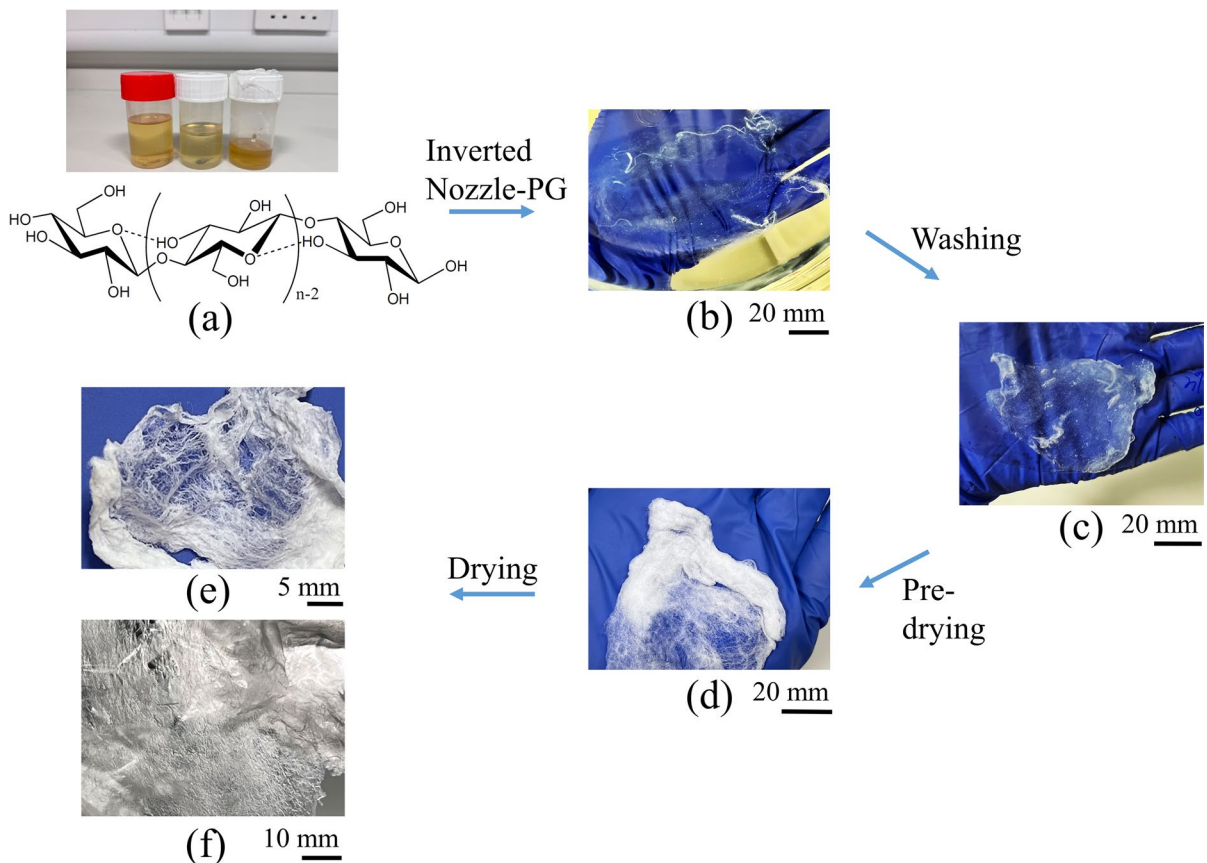


Fig. 2 The preparation process of cellulose fibers/films

at a resolution of 4 cm^{-1} , to obtain a reasonable signal-to-noise ratio. The samples were studied on diamond ATR.

Absorption measurements

The liquid absorption properties of the cellulose samples in PBS solution (pH=7.4) were investigated. Before the experiment, the initial weight of the dry cellulose samples (prepared from 2 wt%, 2.5 wt%, and 3 wt% cellulose solutions, respectively) was measured and denoted as w_0 . Each sample was prepared in three duplications for parallel experiments. The weighed cellulose samples were soaked in the PBS solution and placed in a 37°C incubator. At selected time points, the cellulose samples were removed from the PBS solution and blotted with an absorbent tissue. The weight of the cellulose samples after absorbing liquid was measured and denoted as w_i . The percentage of liquid absorption (W%) of the cellulose samples was calculated according to the following equation:

$$W\% = \frac{w_i - w_0}{w_0} \times 100\%$$

X-ray measurements

X-ray diffraction (XRD) analysis was conducted on different cellulose samples: native cellulose extracted from *Laminaria hyperborea* and three regenerated cellulose samples processed by inverted nozzle-PG, named extracted cellulose, regenerated cellulose (1), regenerated cellulose (2), and regenerated cellulose (3). The measurement was performed on an STOE STADI-P diffractometer (Germany) with a Cu source ($K_{\alpha 1} = 1.5406 \text{ \AA}$ and $K_{\alpha 2} = 1.5444 \text{ \AA}$), using a voltage of 40 kV and a current of 30 mA. The scanning rate was 5s per step with a scanning step of 0.015° . The samples were scanned within the range of 10° – 45° (2θ). The collected data was analyzed using the peak deconvolution method and fitted with the Gaussian function in Origin 2021.

Results and discussion

Solution properties

Surface tension and viscoelasticity are two main factors that determine the solution spinnability in nozzle-PG. Solutions with a very low viscosity cannot provide sufficient chain entanglement to form spinning jets while an extremely viscous solution cannot overcome surface tension, resulting in an inability to form fibers. As shown in Table 1, with the increase of cellulose concentration from 2 to 3 wt%, the solution surface tension and viscosity significantly increased. Within the 1% concentration range, the cellulose solution viscosity increased exponentially from 225 to 22,925 mPa s, and the solution fluidity decreased rapidly. These results exhibited the typical viscosity—concentration dependence of cellulose/EMIM OAc solutions, which is consistent with the previously reported work (Gericke et al. 2009; Quan et al. 2010; Sescousse et al. 2010; Tan et al. 2016). Additionally, the rheological behavior of cellulose/EMIM OAc is affected by the water impurities of the ionic liquid solvent. The water existing in the ionic liquid is considered to decrease the solubility of cellulose, which is presumably due to the competitive hydrogen bonding (Swatloski et al. 2002). Therefore, cellulose extract and ionic liquid are required to be stored in a dry place before use and the dissolution should be processed under conditions that avoid moisture.

*The surface tension data of the 3 wt% cellulose solution was difficult to obtain, due to the influence of the measurement method on the surface tension measurement of highly viscous solutions (Lee et al. 2012).

Table 1 Cellulose solution properties at different polymer concentrations

Solution	wt%	Surface Tension [mN/m]	Viscosity [mPa s]
Cellulose dissolved in EMIM OAc/DMSO	2	50.0 ± 1.3	225.0 ± 6.8
	2.5	65.2 ± 0.5	14377.0 ± 330.5
	3	–	22925.0 ± 1028.9

Regenerated cellulose fibers and films

In this work, the mechanism for making cellulose fibers is essentially a combination of gyro-spinning and wet spinning (dry jet-wet spinning). Inverted nozzle-PG was used to extrude cellulose solutions. The extruded cellulose fluid was stretched in the air to form continuous spinning jets before entering the coagulation bath, due to the pressure difference and fluid viscoelasticity. In the water coagulation bath, the solvent in polymer jets underwent diffusion exchange with the coagulant (a non-solvent with respect to the cellulose). Liquid-liquid phase separation occurred, resulting in gel-like cellulose (Zhang et al. 2005). Meanwhile, intra- and inter-molecular hydrogen bonds of cellulose were re-formed. The cellulose obtained at this stage was a highly swollen gel, which expanded more than its normal size. These cellulose products were much reduced in size after being thoroughly washed and dried. It was found that the swollen gel-like cellulose had a weight ratio of 1500–1800% to the dried cellulose samples, indicating their excellent water retention capacity. Therefore, the morphology and properties of cellulose products were affected by polymer solution properties, system parameters of inverted nozzle-PG, as well as the coagulation process.

Figure 3 exhibits SEM images of cellulose products obtained from 2 wt% (Fig. 3a), 2.5 wt% (Fig. 3b,c), and 3 wt% (Fig. 3d–f) cellulose/EMIM OAc solutions. It's evident that the structure and morphology of the regenerated cellulose products are highly dependent on the solution concentration. Thin films with smooth surfaces were obtained from 2 wt% cellulose solutions. An increase in solution concentration to 2.5 wt% resulted in some large pores presenting on the cellulose products, which simultaneously had fibrous structures and membrane structures with wrinkled surfaces. Continuous interlaced cellulose fibers were spun from the 3 wt% solution. The effect of polymer concentration on the structure and morphology of the regenerated cellulose is mainly through the fluid viscosity during the coagulation process. The low concentration of cellulose substantially reduced the viscosity of cellulose solutions, as discussed in Sect. 3.1. The local mobility around cellulose chains increased due to the low viscosity ratio of the cellulose solution to the coagulant, resulting in a more adequate and faster diffusion of the solvent

and the coagulant, which is beneficial to the even distribution of cellulose molecules (Hedlund et al. 2019). In addition, the lower viscosity solutions generally have shorter relaxation times, suggesting that the polymer jets may have relaxed somewhat before coagulation (Fink et al. 2001). Thus, the 2 wt% cellulose solution was likely to produce homogeneous cellulose films. However, the high viscosity of cellulose solutions hindered the exchange of solvent and coagulant. The coagulant was difficult to diffuse to the central region of the forming fibers, which may result in incomplete phase separation (Makarov et al. 2021). Cellulose tended to retain fibrous structures. In this work, 3 wt% was regarded as the optimal concentration for the formation of continuous cellulose fibers.

Besides, solution concentration influences the optical properties of cellulose products obtained. The low concentration (2 wt%) of cellulose solution led to cellulose films with good optical transmittance (Fig. 2f), whereas conventional cellulose fibers with inferior transmittance were produced by the 3 wt% solutions (Fig. 2e). The optical transmittance is mainly affected by the homogeneous structure of the cellulose samples rather than the thickness (Liu and Zhang 2009). Previous studies have reported that, due to different phase separation processes, cellulose films with homogeneous structures were generally formed by lower cellulose concentrations, while higher concentrations resulted in more compact but in-homogeneous structures in cellulose products (Cai et al. 2007; Liu and Zhang 2009).

The effect of air gap length (collection distance) is shown in Fig. 3d–i. According to a previous report (Dai et al. 2022), increasing collection distance facilitates the stretching and thinning of the polymer jets in the air to form finer fibers. In this study, the cellulose fiber diameter decreased from 8.0 ± 3.4 to 5.6 ± 2.5 μm with the increase in collection distance from 6 to 13 mm. While the fiber diameter increased to 7.5 ± 3.5 μm when the collection distance was further increased to 20 mm. This can be explained by the longer relaxation time at a longer air gap. The polymer jets underwent a longer relaxation time and expanded more at the 20 mm distance than those at a shorter distance, resulting in thicker fibers. A similar phenomenon can be seen from the spinning of 2.5 wt% cellulose solution. Some fibrous structures were presented on the cellulose products that were collected at the 6 mm distance (Fig. 3b), while only

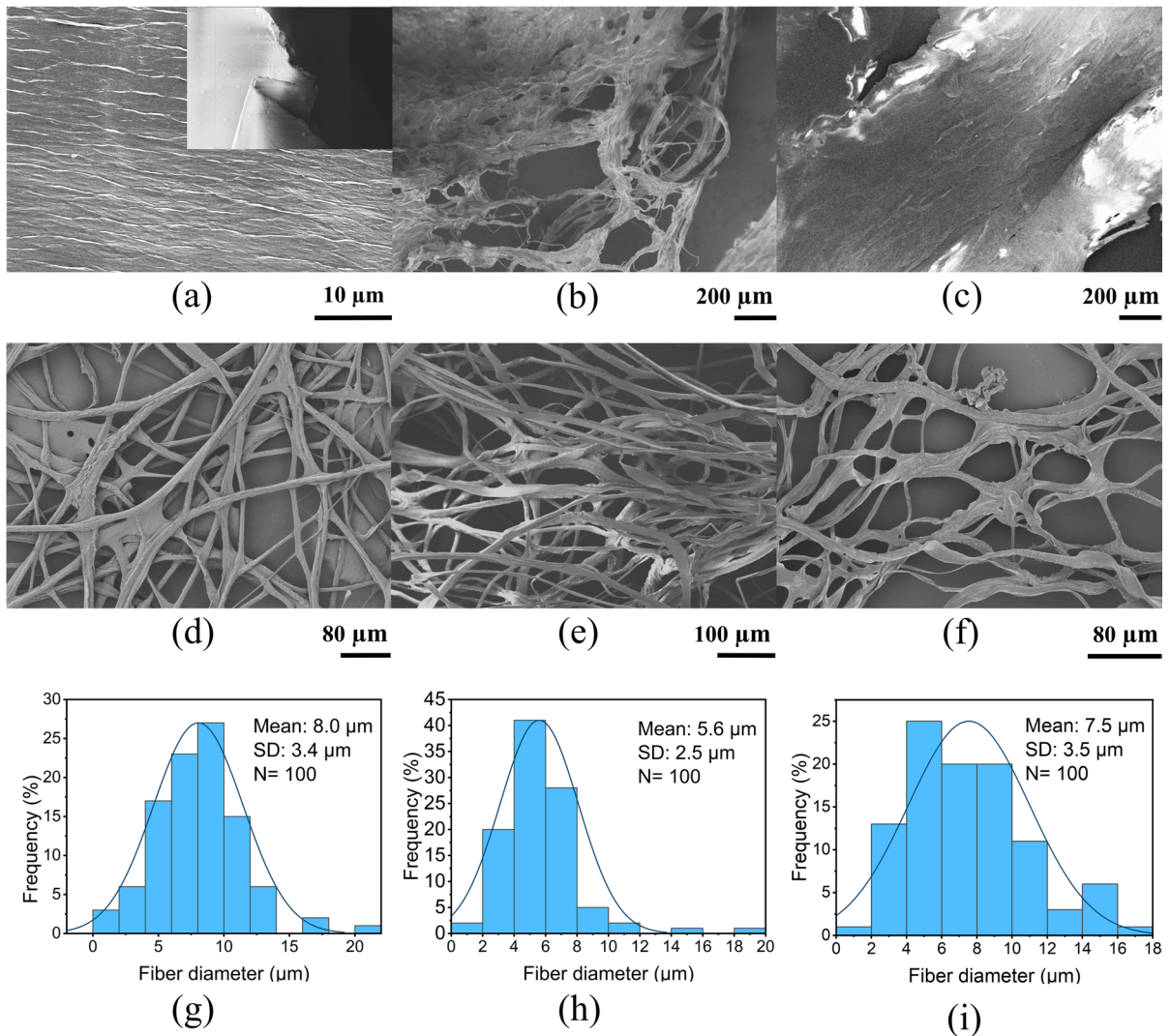


Fig. 3 SEM images of cellulose processed by inverted nozzle-PG at 0.1 MPa working pressure: **a** 2 wt% cellulose, 6 mm distance; **b**, **c** 2.5 wt% cellulose, 6 and 13 mm distance, respec-

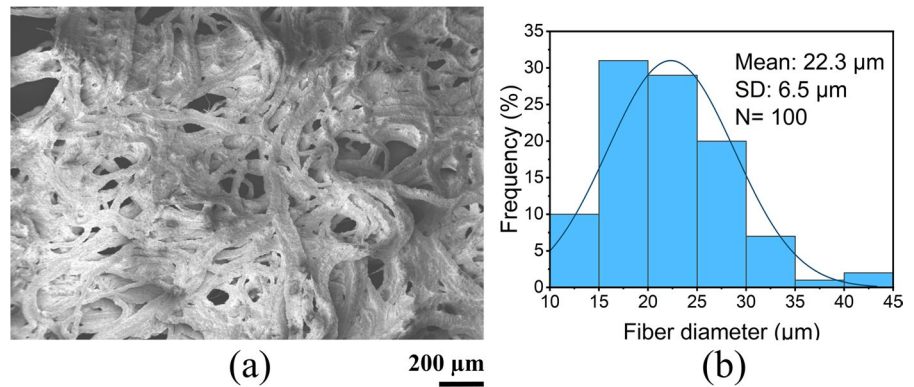
tively; **d–f** 3 wt% cellulose, 6 mm, 13 and 20 mm distance, respectively. **g–h** diameter distributions of cellulose fibers collected at 6 mm, 13 and 20 mm, respectively

wide ribbon-like cellulose was obtained from the 13 mm collection distance (Fig. 3c). Therefore, the influence of air gap length on the morphology of cellulose products is a synergistic result of jet stretching and relaxation. A trade-off between the two is conducive to obtaining finer fibers. In addition, the air gap conditions (temperature, humidity) were reported to affect the cellulose fiber formation, which needs to be investigated in future work (Fink et al. 2001).

It was found that the magnitude of the working pressure applied in inverted nozzle-PG also

affected the fiber morphology. When the pressure was increased to 0.2 MPa, the obtained cellulose product had fibrous textures but there was significant aggregation (Fig. 4a). This can be attributed to the kinetic instability and insufficient stretching time of the polymer jets caused by the high-velocity gas flow. Moreover, the fiber diameter increased to $22.3 \pm 6.5 \mu\text{m}$, which is much larger than those fibers obtained from the spinning at 0.1 MPa. The large diameter value acquired in this case can be the result of insufficient stretching or/and an artifact of fiber aggregation.

Fig. 4 **a** SEM image and **b** diameter distribution of 3 wt% cellulose solution processed by inverted nozzle-PG at 0.2 MPa working pressure and 13 mm distance



However, the effect of increasing pressure is not always negative. The results showed that the production rate of cellulose fibers increased from 17.6 g/h to 21.6 g/h, indicating that the higher pressure played a role in promoting fiber formation in this work.

Figure 5 shows that the cellulose films have flat and relatively smooth surfaces while the cellulose fibers have distinctly wrinkled surfaces. The smooth surface of the cellulose films can be attributed to the better fluidity and the fast liquid fusion of low-viscous solutions as discussed previously. The collapsed and wrinkled surfaces of the cellulose fibers are attributed to the coagulation and drying processes. It has been discussed that the high viscoelasticity of the cellulose solution hindered the non-solvent (coagulant) from entering the central region of fibers while the surface of fibers coagulated. The volume of dried fibers was significantly reduced compared to swollen fibers. The different contraction rates of the fiber surface and the fiber core during the drying process can cause wrinkles and collapse of the fibers.

Absorption properties of cellulose fibers and films

Figure 6 exhibits the liquid absorption capacity of cellulose samples with different morphologies in PBS solutions. Within the initial 10 h, the three cellulose samples all showed a high liquid absorption rate. At the 8.5th hour after soaking, the cellulose films prepared from the 2 wt% solution had an absorption percentage of $183 \pm 23\%$, while the absorption percentage of fibrous cellulose obtained from the higher concentration solutions reached 210%. Ultimately, cellulose samples prepared from the 2 wt%, 2.5 wt%, and 3 wt% solutions reached the saturation level having a maximum absorption capacity of $192 \pm 21\%$, $212 \pm 6\%$, and $248 \pm 29\%$, respectively. The cellulose fibers showed higher liquid absorption capacity compared to the cellulose films, which may be attributed to the higher surface area-to-volume ratio of fibrous samples. The hydrophilic properties of cellulose materials are due to the formation of hydrogen bonds between their hydroxyl groups and water molecules

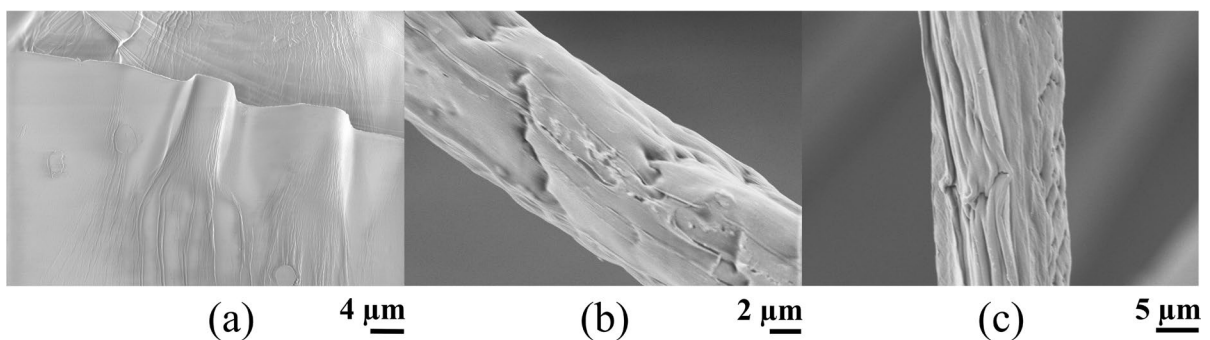


Fig. 5 The surface topography of **a** cellulose film and **b, c** cellulose fibers

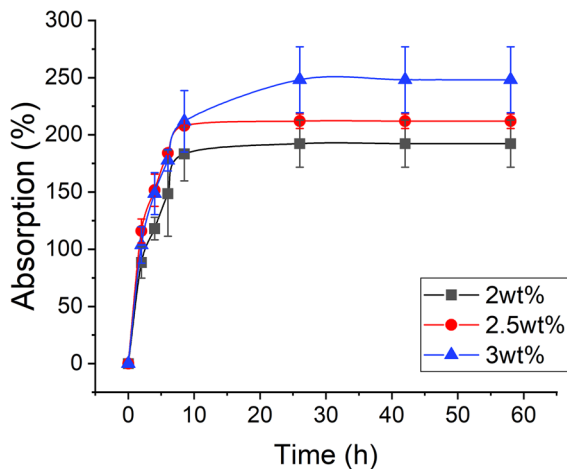


Fig. 6 Absorption capacity of the obtained cellulose samples

(Alamri and Low 2012). This unique hydration ability of cellulose provides a moist environment desired for wound healing, making it an attractive material for wound bandages (Lin et al. 2013; Miao et al. 2011).

Fourier transform infrared spectroscopy

FTIR spectroscopy was used to verify the chemical composition of cellulose molecules. Based on Fig. 7, the FTIR spectrums of cellulose samples produced by different solution concentrations showed

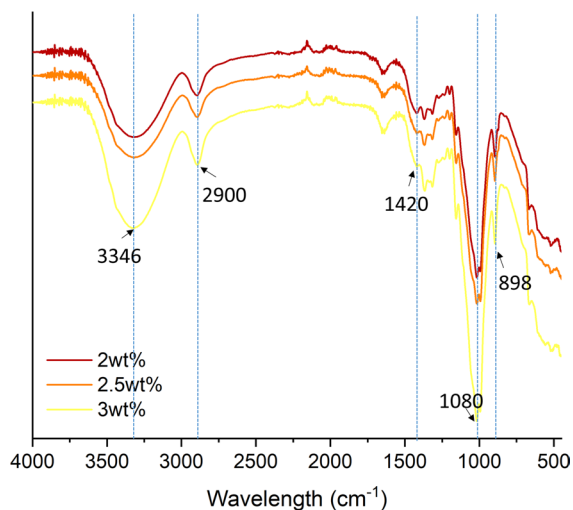


Fig. 7 FTIR spectra of cellulose samples obtained from different polymer concentrations

similar absorption characteristics. The broad absorption peak at 3346 cm^{-1} is attributed to the stretching vibration of O–H. This peak also includes inter- and intra-molecular hydrogen bond vibrations in cellulose (Popescu et al. 2011). The absorption peak of 2900 cm^{-1} and 1080 cm^{-1} are characteristics of C–H and C–O bonds stretching vibrations, respectively. The band around $1420\text{--}1430\text{ cm}^{-1}$ can be used to analyze the crystallinity of cellulose, while the band of 898 cm^{-1} is assigned to amorphous regions in cellulose (Poletto et al. 2014). According to O’Conner et al. (Nelson and O’Connor 1964), the spectral ratio of $1429/893\text{ cm}^{-1}$ can be defined as the crystallinity index of cellulose samples.

X-ray diffraction

The XRD diffractogram (Fig. 8) clearly showed distinct differences in the crystallization behavior between the extracted cellulose and regenerated cellulose samples. In the case of cellulose extracted from *Laminaria hyperborea*, the diffraction pattern exhibited characteristic peaks at $2\theta = 14.4^\circ$, 16.7° , 22.7° , and 34.6° , which have been identified as corresponding to the (100), (010), (110), and (11–4) crystallographic planes for cellulose I (French 2014). Based on Bragg’s law, the d-spacing data acquired through X-ray diffractometry were utilized in the discriminant analysis function proposed by Wada et al. (2001). The analysis revealed that the

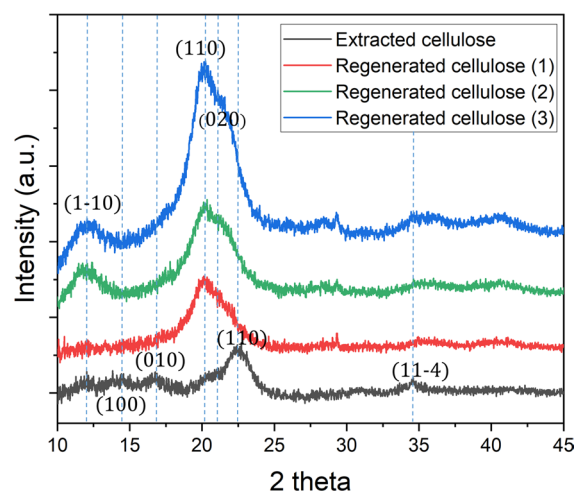


Fig. 8 X-ray diffractograms of extracted cellulose and regenerated cellulose

extracted cellulose predominantly belongs to the I_{α} -rich type. These results are consistent with the previous study, using the same *Laminaria hyperborea* source material identified as Cellulose I_{α} (Onyianta et al. 2020). Whereas the peaks at $2\theta = 12.0^{\circ}$, 20.2° , and 21.1° observed in the diffraction patterns of regenerated cellulose in this work were indicative of the (1–10), (110), and (020) crystallographic planes of cellulose II (French 2014). The change in crystallography suggests that cellulose I converted into cellulose II after the regeneration process, due to the breaking and rebuilding of hydrogen bonds of cellulose molecules in ionic liquids (Liu et al. 2021). The hydrogen bonds in cellulose I are organized in a sheet array in (020) planes (Gardner and Blackwell 1974) while there is a three-dimensional network of hydrogen bonds in cellulose II (Langan et al. 1999). The conversion from cellulose I to cellulose II is an irreversible process. Cellulose II is commonly acknowledged as a stable crystalline form of cellulose (Habibi et al. 2010).

To evaluate the changes in cellulose molecular orientation after the regeneration process, orientation index (OI) was used to quantify this material characteristic. OI was defined as Eq. 1 (Croitoru and Patachia 2014):

$$OI = 1 - \frac{I_{am}}{I_{tot}} \quad (1)$$

where I_{am} is the maximum intensity of the peak corresponding to the dominating amorphous fractions, and I_{tot} is the maximum intensity of the diffraction pattern. OI ranges from 0 to 1. A higher value suggests a more aligned molecular chain orientation, whereas $OI = 0$ signifies a completely random orientation.

The calculated results show that the extracted cellulose has an OI of 0.91, aligning with the anticipated preferred orientation seen in natural cellulose I_{α} (Onyianta et al. 2020). However, the regenerated cellulose, processed under different parameters, displays an average OI of 0.39 ± 0.09 . As previously highlighted, dissolution in ionic liquids leads to the breakage and reconstruction of hydrogen bonds in cellulose chains, resulting in the conversion of cellulose from type I to type II, which is marked by a reduced orientation. Variations in orientation among different regenerated cellulose might be attributed to disparate processing conditions during the spinning process.

Conclusions

Cellulose is an ecologically sustainable material that possesses inherent biocompatibility and biodegradability, rendering it a highly promising candidate for numerous industrial and biomedical applications. In this study, thin cellulose film sheets exhibiting favorable optical properties and well-defined cellulose fibers with a diameter of approximately $5 \mu\text{m}$ were manufactured via the advanced technology of inverted nozzle-pressurized gyration combined with wet spinning. This method broadens the range of processing strategies for cellulose and effectively addresses the existing challenges associated with the widespread use of cellulose materials. Given the similar properties and processing techniques of some biomaterials, the technique of inverted nozzle-pressurized gyration is expected to be applicable to other biopolymers, such as sodium alginate.

Acknowledgements The authors thank the UCL Mechanical Engineering workshop led by Peter Kelly for the significant contributions to the construction of the spinning vessels. The authors are also grateful to Dr Fei Peng for supporting the microscopic imaging. YD is supported by the China Scholarship Council (CSC) for her PhD studies at University College London. We thank UKRI for funding the core pressurized gyration research at UCL (Grants: EP/S016872/1, EP/N034228/1, EP/L023059/1). We also like to thank Prof. Alfred D. French for his advice on the characterization aspects of this work.

Author contributions YD: methodology, investigation, formal analysis, writing—original draft. DS, SS, DO, MD: resources, writing—reviewing. AD: methodology. ME: supervision, visualization, conceptualization, writing—reviewing.

Funding Not applicable.

Data availability All relevant data are within the manuscript and its supplementary information file and are available from the corresponding author upon reasonable request.

Declarations

Conflict of interest The authors declare that they have no conflict of interest.

Ethical approval Not applicable.

Consent for publication Not applicable.

Open Access This article is licensed under a Creative Commons Attribution 4.0 International License, which permits use, sharing, adaptation, distribution and reproduction in any medium or format, as long as you give appropriate credit to the

original author(s) and the source, provide a link to the Creative Commons licence, and indicate if changes were made. The images or other third party material in this article are included in the article's Creative Commons licence, unless indicated otherwise in a credit line to the material. If material is not included in the article's Creative Commons licence and your intended use is not permitted by statutory regulation or exceeds the permitted use, you will need to obtain permission directly from the copyright holder. To view a copy of this licence, visit <http://creativecommons.org/licenses/by/4.0/>.

References

- Alamri H, Low IM (2012) Mechanical properties and water absorption behaviour of recycled cellulose fibre reinforced epoxy composites. *Polym Test* 31(5):620–628. <https://doi.org/10.1016/j.polymertesting.2012.04.002>
- Cai J, Wang LX, Zhang LN (2007) Influence of coagulation temperature on pore size and properties of cellulose membranes prepared from NaOH-urea aqueous solution. *Cellulose* 14(3):205–215. <https://doi.org/10.1007/s10570-007-9106-3>
- Croitoru C, Patachia S (2014) Biocomposites obtained from wood saw dust using ionic liquids. *Acta Chem Iasi* 22(2):113–134
- Dai Y, Ahmed J, Delbusso A, Edirisinghe M (2022) Nozzle-pressurized gyration: a novel fiber manufacturing process. *Macromol Mater Eng* 307(9):2200268. <https://doi.org/10.1002/mame.202200268>
- Dai Y, Ahmed J, Edirisinghe M (2023) Pressurized gyration: fundamentals, advancements, and future. *Macromol Mater Eng* 308(7):2300033. <https://doi.org/10.1002/mame.202300033>
- Durmaz EN, Çulfaz-Emecen PZ (2018) Cellulose-based membranes via phase inversion using [EMIM]OAc-DMSO mixtures as solvent. *Chem Eng Sci* 178:93–103. <https://doi.org/10.1016/j.ces.2017.12.020>
- Elschner T, Köteritzsch M, Heinze T (2014) Synthesis of cellulose tricarbonates in 1-butyl-3-methylimidazolium chloride/pyridine. *Macromol Biosci* 14(2):161–165. <https://doi.org/10.1002/mabi.201300345>
- Fink HP, Weigel P, Purz H, Ganster J (2001) Structure formation of regenerated cellulose materials from NMMO-solutions. *Prog Polym Sci* 26(9):1473–1524
- French AD (2014) Idealized powder diffraction patterns for cellulose polymorphs. *Cellulose* 21(2):885–896. <https://doi.org/10.1007/s10570-013-0030-4>
- Gardner KH, Blackwell J (1974) The structure of native cellulose. *Biopolymers* 13(10):1975–2001. <https://doi.org/10.1002/bip.1974.360131005>
- Gericke M, Schlufker K, Liebert T, Heinze T, Budtova T (2009) Rheological properties of cellulose/ionic liquid solutions: from dilute to concentrated states. *Biomacromolecules* 10(5):1188–1194
- Habibi Y, Lucia LA, Rojas OJ (2010) Cellulose nanocrystals: chemistry, self-assembly, and applications. *Chem Rev* 110(6):3479–3500
- Haerens K, Deuren SV, Matthijs E, Bruggen BVD (2010) Challenges for recycling ionic liquids by using pressure driven membrane processes. *Green Chem* 12(12):2182–2188
- Handy ST, Zhang X (2001) Organic synthesis in ionic liquids: the Stille coupling. *Org Lett* 3(2):233–236
- Hedlund A, Kohnke T, Hagman J, Olsson U, Theliander H (2019) Microstructures of cellulose coagulated in water and alcohols from 1-ethyl-3-methylimidazolium acetate: contrasting coagulation mechanisms. *Cellulose* 26(3):1545–1563. <https://doi.org/10.1007/s10570-018-2168-6>
- Heseltine PL, Ahmed J, Edirisinghe M (2018) Developments in pressurized gyration for the mass production of polymeric fibers. *Macromol Mater Eng* 303(9):1800218. <https://doi.org/10.1002/mame.201800218>
- Holbrey JD, Seddon KR (1999) Ionic liquids. *Clean Prod Process* 1(4):223–236. <https://doi.org/10.1007/s100980050036>
- Klemm D, Heublein B, Fink HP, Bohn A (2005) Cellulose: fascinating biopolymer and sustainable raw material. *Angew Chem Int Ed* 44(22):3358–3393. <https://doi.org/10.1002/anie.200460587>
- Langan P, Nishiyama Y, Chanzy H (1999) A revised structure and hydrogen-bonding system in cellulose II from a neutron fiber diffraction analysis. *J Am Chem Soc* 121(43):9940–9946
- Lee BB, Chan ES, Ravindra P, Khan TA (2012) Surface tension of viscous biopolymer solutions measured using the Du Nouy ring method and the drop weight methods. *Polym Bull* 69(4):471–489
- Li W, Jin A, Liu C, Sun R, Zhang A, Kennedy J (2009) Homogeneous modification of cellulose with succinic anhydride in ionic liquid using 4-dimethylaminopyridine as a catalyst. *Carbohydr Polym* 78(3):389–395
- Lin N, Dufresne A (2014) Nanocellulose in biomedicine: current status and future prospect. *Eur Polym J* 59:302–325
- Lin WC, Lien CC, Yeh HJ, Yu CM, Hsu SH (2013) Bacterial cellulose and bacterial cellulose–chitosan membranes for wound dressing applications. *Carbohydr Polym* 94(1):603–611. <https://doi.org/10.1016/j.carbpol.2013.01.076>
- Liu SL, Zhang LN (2009) Effects of Polymer concentration and coagulation temperature on the properties of regenerated cellulose films prepared from LiOH/urea solution. *Cellulose* 16(2):189–198. <https://doi.org/10.1007/s10570-008-9268-7>
- Liu X, Pang J, Zhang X, Wu Y, Sun R (2013) Regenerated cellulose film with enhanced tensile strength prepared with ionic liquid 1-ethyl-3-methylimidazolium acetate (EMIMAc). *Cellulose* 20:1391–1399. <https://doi.org/10.1007/s10570-013-9925-3>
- Liu Y, Jing S, Carvalho D, Fu J, Martins M, Cavaco-Paulo A (2021) Cellulose dissolved in ionic liquids for modification of the shape of keratin fibers. *ACS Sustain Chem Eng* 9(11):4102–4110
- Mahalingam S, Edirisinghe M (2013) Forming of polymer nanofibers by a pressurised gyration process. *Macromol Rapid Commun* 34(14):1134–1139. <https://doi.org/10.1002/marc.201300339>
- Makarov IS, Golova LK, Vinogradov MI et al (2021) Morphological transformations in the process of coagulation

- of cellulose solution in N-methylmorpholine N-oxide with isobutanol. *Polym Sci Ser C* 63(2):161–169
- McCormick CL, Callais PA, Hutchinson BH Jr (1985) Solution studies of cellulose in lithium chloride and *N,N*-dimethylacetamide. *Macromolecules* 18(12):2394–2401. <https://doi.org/10.1021/ma00154a010>
- Miao J, Pangule RC, Paskaleva EE et al (2011) Lysostaphin-functionalized cellulose fibers with antistaphylococcal activity for wound healing applications. *Biomaterials* 32(36):9557–9567. <https://doi.org/10.1016/j.biomaterials.2011.08.080>
- Michud A, Tanttu M, Asaadi S et al (2016) Ioncell-F: ionic liquid-based cellulosic textile fibers as an alternative to viscose and Lyocell. *Text Res J* 86(5):543–552
- Nelson ML, O'Connor RT (1964) Relation of certain infrared bands to cellulose crystallinity and crystal lattice type. Part II. A new infrared ratio for estimation of crystallinity in celluloses I and II. *J Appl Polym Sci* 8(3):1325–1341. <https://doi.org/10.1002/app.1964.070080323>
- Onyianta AJ, O'Rourke D, Sun D, Popescu CM, Dorris M (2020) High aspect ratio cellulose nanofibrils from macroalgae *Laminaria hyperborea* cellulose extract via a zero-waste low energy process. *Cellulose* 27(14):7997–8010. <https://doi.org/10.1007/s10570-020-03223-5>
- Pinkert A, Marsh KN, Pang S, Staiger MP (2009) Ionic liquids and their interaction with cellulose. *Chem Rev* 109(12):6712–6728
- Poletto M, Ornaghi HL, Zattera AJ (2014) Native cellulose: structure, characterization and thermal properties. *Materials* 7(9):6105–6119
- Popescu MC, Popescu CM, Lisa G, Sakata Y (2011) Evaluation of morphological and chemical aspects of different wood species by spectroscopy and thermal methods. *J Mol Struct* 988(1):65–72. <https://doi.org/10.1016/j.molstruc.2010.12.004>
- Quan SL, Kang SG, Chin IJ (2010) Characterization of cellulose fibers electrospun using ionic liquid. *Cellulose* 17(2):223–230. <https://doi.org/10.1007/s10570-009-9386-x>
- Salama A, Hesemann P (2020) Recent trends in elaboration, processing, and derivatization of cellulosic materials using ionic liquids. *ACS Sustain Chem Eng* 8(49):17893–17907
- Sayyed AJ, Deshmukh NA, Pinjari DV (2019) A critical review of manufacturing processes used in regenerated cellulosic fibres: viscose, cellulose acetate, cuprammonium, LiCl/DMAc, ionic liquids, and NMMO based lyocell. *Cellulose* 26(5):2913–2940. <https://doi.org/10.1007/s10570-019-02318-y>
- Seddiqi H, Oliaei E, Honarkar H et al (2021) Cellulose and its derivatives: towards biomedical applications. *Cellulose* 28(4):1893–1931. <https://doi.org/10.1007/s10570-020-03674-w>
- Sescousse R, Le KA, Ries ME, Budtova T (2010) Viscosity of cellulose-imidazolium-based ionic liquid solutions. *J Phys Chem B* 114(21):7222–7228
- Swatloski RP, Spear SK, Holbrey JD, Rogers RD (2002) Dissolution of cellose with ionic liquids. *J Am Chem Soc* 124(18):4974–4975
- Tan X, Li X, Chen L, Xie F (2016) Solubility of starch and microcrystalline cellulose in 1-ethyl-3-methylimidazolium acetate ionic liquid and solution rheological properties. *Phys Chem Chem Phys* 18(39):27584–27593
- Wada M, Okano T, Sugiyama J (2001) Allomorphs of native crystalline cellulose I evaluated by two equatorial-d spacings. *J Wood Sci* 47(2):124–128
- Wang X, Li H, Cao Y, Tang Q (2011) Cellulose extraction from wood chip in an ionic liquid 1-allyl-3-methylimidazolium chloride (AmimCl). *Bioresour Technol* 102(17):7959–7965. <https://doi.org/10.1016/j.biortech.2011.05.064>
- Wang H, Gurau G, Rogers RD (2012) Ionic liquid processing of cellulose. *Chem Soc Rev* 41(4):1519–1537
- Wu B, Liu W, Zhang Y, Wang H (2009) Do we understand the recyclability of ionic liquids? *Chem Eur J* 15(8):1804–1810. <https://doi.org/10.1002/chem.200801509>
- Zhang L, Mao Y, Zhou JP, Cai J (2005) Effects of coagulation conditions on the properties of regenerated cellulose films prepared in NaOH/urea aqueous solution. *Ind Eng Chem Res* 44(3):522–529
- Zhu S, Wu Y, Chen Q et al (2006) Dissolution of cellulose with ionic liquids and its application: a mini-review. *Green Chem* 8(4):325–327
- Zhuang X, Yang X, Shi L, Cheng B, Guan K, Kang W (2012) Solution blowing of submicron-scale cellulose fibers. *Carbohydr Polym* 90(2):982–987

Publisher's Note Springer Nature remains neutral with regard to jurisdictional claims in published maps and institutional affiliations.